Experimental Detection of Oxygenated Aromatics in an Anisole Blended Flame

Kanika Sood, Sylvie Gosselin, Seifali Mehrdad, Nathalie de Coensel, Juan Carlos Lizardo Huerta, Abderrahman El Bakali, Kevin M van Geem, Laurent Gasnot, Luc-Sy Tran

Published in Energy & Fuels
https://doi.org/10.1021/acs.energyfuels.3c04800

Experimental Detection of Oxygenated Aromatics in an Anisole Blended Flame

*Kanika Sood[1], Sylvie Gosselin[1], Mehrdad Seifali Abbas-Abadi[2], Nathalie De Coensel[2], Juan-Carlos Lizardo-Huerta[1], Abderrahman El Bakali[1], Kevin M. Van Geem[2], Laurent Gasnot[1], Luc-Sy Tran[1,] **

[1] Univ. Lille, CNRS, UMR 8522 - PC2A - Physicochimie des Processus de Combustion et de l'Atmosphère, F-59000 Lille, France.
[2] Laboratory for Chemical Technology (LCT), Ghent University, Technologiepark 125, B-9052 Ghent, Belgium.

KEYWORDS: Combustion, flame, lignin-based biofuels, anisole, oxygenated aromatics, GC-MS

*** Corresponding author:** Dr. Luc-Sy Tran. E-mail: luc-sy.tran@univ-lille.fr

ABSTRACT

Anisole serves as a pivotal constituent in the model for lignin-derived biofuels. Despite the considerable interest in these biofuels, their combustion processes have the potential to increase the formation of aromatic compounds, particularly oxygenated aromatics. These oxygen-containing aromatics, known for their increased toxicity compared to conventional aromatics, can significantly impact the characteristics of soot particles and exhaust gas emissions. Recent research efforts have delved into the formation of oxygenated aromatics during combustion. However, the understanding of the kinetics governing the production of these aromatics remains limited, primarily due to a scarcity of experimental data for their identification. This study addresses this gap by investigating a fuel-rich hydrocarbon flame enriched with 10% anisole at an equivalence ratio of 1.90 and atmospheric pressure. Chemical products sampled from the flame underwent analysis using 1D and 2D Gas Chromatography-Mass Spectrometry setups. The results facilitated the separation and identification of over 100 aromatic species, encompassing approximately 80 oxygenated variants with diverse functional groups such as alcohols, ethers, carbonyls (aldehydes, ketones), and esters. The molecular weights of these species ranged from 94 (phenol) to 224 (9-fluorenyl acetate). Surprisingly, only a fraction of the identified species has been considered in existing literature models. Notably, alcohol and ether functional groups emerged as the most prevalent among the detected aromatics, hinting at their crucial roles in the reaction mechanisms involving anisole. The dominant reaction paths are identified and discussed in detail, offering valuable insights for future enhancements of kinetic models pertaining to "lignin-based biofuel and oxygenated aromatics”.

TOC GRAPHIC

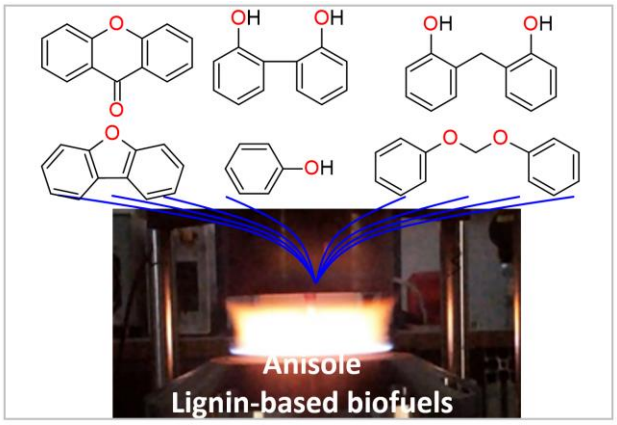

1. INTRODUCTION

Currently, around 80% of the energy production comes from the combustion of fossil fuels [1]. Research interests have shifted towards exploring environment friendly alternative fuels with the intercontinental awareness and recognition of energy and environmental concerns. Biofuels produced from biomass are being considered as vital parts of the sustainable energy panel, where they promise to contribute to our society's energy security [2,3]. Lignin is one of the main components of biomass, and its structure contains a large portion of aromatic rings with oxygen functionalities such as the hydroxyl and methoxy groups [4–6]. Though it has been considered as a by-product during the paper pulping process as well as in the production of cellulosic ethanol, recent research has shown that lignin can be converted, via different processes, into a variety of valuable chemicals and fuels (called "lignin-based biofuels") [4,5,7,8]. Despite the undeniable interest presented by these biofuels, their combustion processes are likely to elevate the formation of aromatic species, especially oxygenated aromatics including oxygenated polycyclic aromatic hydrocarbons (OPAHs), that may profoundly modify the properties of the pollutant emissions [9–11]. There is increasing evidence that OPAHs are more toxic than their parent PAH analogs [12–17]. It has also been reported that OPAHs are more persistent in the environment as opposed to other organic compounds [12,18,19]. Understanding the formation kinetics of OPAHs in the combustion of lignin-based biofuels should be thus crucial.

Anisole was recently investigated as a component model of lignin-based biofuels or bio-oils [20–22]. It was chosen as fuel in the present study. Anisole owns to its suitable properties for internal combustion engines, for instance, a high octane number (RON=114) and a high lower heating value (33 MJ/L) that is superior than that of ethanol (21.3 MJ/L) and similar to that of gasoline (30.1-33.3 MJ/L) [20,23]. Since recent years, anisole combustion has been a subject of interest for numerous fundamental investigations focusing on ignition delay times, laminar flame velocity, chemical species from combustion/pyrolysis, and soot formation [21,22,24–29,29–36]. However, studies focusing on the experimental detection of oxygenated aromatics and OPAHs from the oxidation of this fuel are still very scarce in the literature. Though some OPAHs have been experimentally identified in anisole combustion in the literature studies, it is worth mentioning that the species analyzed so far are rather limited to mainly benzofuran and dibenzofuran [22,27,30,31,33,37]. Amongst these studies, there are only two studies in flame conditions [27,33]. Recently, Chen et al. [37] investigated anisole oxidation in a jet stirred reactor coupled to molecular beam mass spectrometry and reported about 40 signals corresponding to the mass of OPAHs (inferring the overall chemical formulae of OPAHs). This study of Chen et al. [37] can be considered as an important contribution to the ongoing advancement in the investigation of OPAH kinetics from anisole oxidation. Though overall chemical formulae were

proposed, a thermodynamic approach (based on the determination of the Gibbs free energies) was used to elucidate the most probable chemical structures corresponding to each of these formulae. It is however important to note that the results using this approach are valid only if the species is present in the real samples, as low Gibbs free energy does not certainly imply that a given species could be produced during the combustion of anisole because of kinetic limitations, thus resulting in dubious and skeptical identification. As also mentioned by Chen et al. [37], the distinct structures of many OPAHs could not be identified because of many isomeric possibilities, especially for isomers with close Gibbs free energies.

Motivated (i) by the importance of OPAHs formed during the combustion of lignin-based biofuels (promising source of renewable fuel), (ii) by the lack of experimental data for OPAHs under flame conditions, and (iii) by the acute challenges associated with the experimental identification of isomeric OPAHs recently narrated in the literature we performed this study and report evidences concerning experimental identification of oxygenated aromatics in an anisole blended flame.

2. EXPERIMENTAL METHOD

A laminar premixed flame burner coupled to a dual-liquid-fuel system and different Gas Chromatography-Mass Spectrometry (GC-MS) setups were used to carry out this work. A schematic representation of the overall experimental setup together with the analytical system is shown in Figure 1. These setups have been described in the subsequent sections.

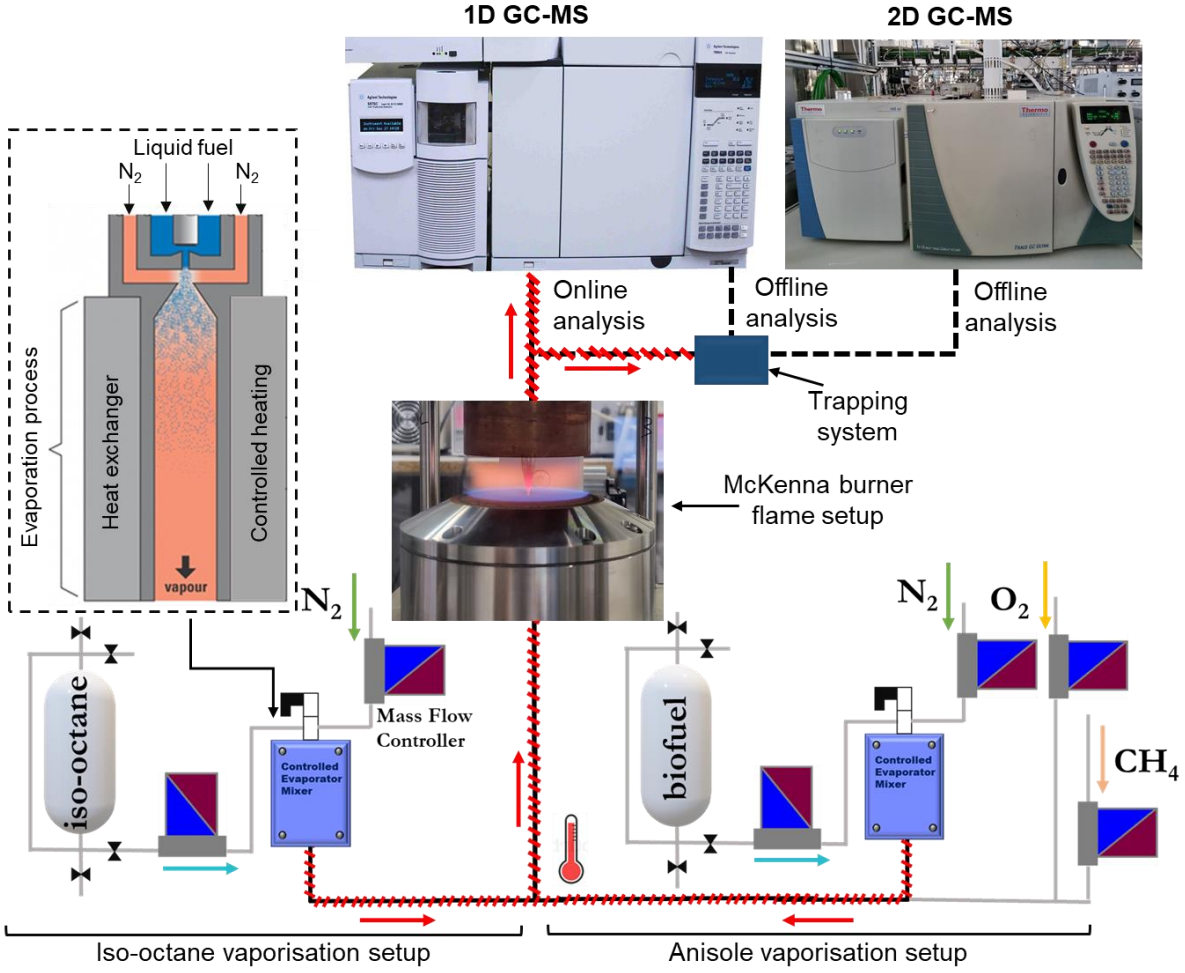

Figure 1. A pictorial representation of the laminar premixed flame burner coupled to the dual-liquid-fuel vaporisation system (together with the depiction of the liquid fuel vaporisation step) and the analytical system used for identification of oxygenated aromatics.

2.1. Flame Burner Setup and Flame Conditions

The liquid flow rates of anisole (Sigma-Aldrich, purity 99.0%) and iso-octane (Sigma-Aldrich, purity 99.0%) were controlled by a dual-liquid system. This system is constituted of two Coriolis mass flow controllers (Bronkhorst, error ±0.2%) followed by two evaporators/mixers, in which liquid fuels were nebulized, vaporized, and mixed with N_2. The gaseous stream was then mixed with O_2 and CH_4 and then fed to the burner. A pictorial representation of the evaporation process is depicted in Figure 1. Flow rates of CH_4 (Air Liquide, purity ≥99.95%), O_2 (Air Liquide, purity ≥ 99.995%) and N_2 (Air Liquide, purity ≥ 99.995%) were controlled using mass flow controllers (Bronkhorst, error ±0.5%).

A flame of iso-octane/methane doped with 10% anisole (*vs* fuel mixture) was stabilized on a McKenna flat flame burner at atmospheric pressure with an equivalence ratio of 1.90 and a total flow rate of 9.86 L_n/min. Methane was necessary to stabilize the flame. 10% anisole addition to a reference fuel was chosen instead of using neat anisole due to the general range of biofuel-gasoline blends that are currently used in real commercial applications. Iso-octane was chosen as a base liquid hydrocarbon fuel because it is commonly used as a representative branched alkane and is one of the main components in gasoline surrogates [38–40]. The ratio of anisole/iso-octane/methane/O_2/N_2 in initial gas phase mixture introduced into the flame is 1.06%/1.56%/8.00%/23.42%/65.96%. In this flame, 71.3% of the carbon is from iso-octane and anisole, and 28.7% comes from methane. The burner system is similar to that described previously in Ref [41]. A schematic figure of the burner is available in the Supporting Information (Figure S1). The central porous zone of the burner (60 mm in diameter) is surrounded by another co-annular porous used for the nitrogen shroud (25 L_n/min), which makes it possible to avoid the air entrainment responsible for the formation of a peripheral or an external diffusion flame. The temperature of the burner is constantly maintained at 60°C using a cryostat. To stabilize fuel-rich flames, a stainless-steel disc, also known as the stagnation plate (6 cm in diameter and 3 cm thick) was surmounted at 21 mm with respect to the burner surface to stabilize the flame away from the burner surface, and was pierced at its center to provide access for the sampling probe. An additional metallic grid was placed directly on the stagnation plate, to avoid peripherical flame ignition. The burner could be vertically displaced with respect to the probe in order to effectuate the sampling process at different heights above the burner (HAB).

2.2. Gas Chromatography Systems

Gas samples were extracted from the flame and directed to the sampling heated line via a quartz probe with an orifice diameter of about 190 µm. The sampling line is connected either directly to a 1D GC-MS for online analyses for abundant aromatics or a liquid N_2 trapping system for offline analyses for relatively less abundant aromatics and for 2D GC-MS experiments, which are described subsequently. Aromatics were identified on account of their individual retention times and distinct mass spectrometry spectra, which were obtained from one 1D GC at PC2A (PhysicoChimie des Processus de Combustion et de l'Atmosphère), Lille and one 2D GC at LCT (Laboratory for Chemical Technology), Ghent. Different split ratios for the GC injectors and samples at different HABs were used to resolve the complex mixtures of flame samples for exhaustive identification of species.

The 1D GC is equipped with a quadrupole mass spectrometer with electron ionization at 70 eV (Agilent Technologies 5975C). MS involves transforming components of a sample into ions, accelerating them by an electric field, and separating ions with different mass-to-charge (m/z) ratios. The obtained mass spectrum was compared with spectral libraries from the NIST-MS database [42] and pure-product injections when possible. Two chromatographic columns with helium as the carrier gas were alternatively used. The first column is the Rt-Q Bond 30m×0.25mm×8µm, nonpolar column, which incorporates 100% divinylbenzene and was used to analyze smaller aromatics. The second column is the SCION-17MS 30m×0.32mm×0.25µm, which is a medium polar column incorporating 50% phenyl methylpolysiloxane and was used

to investigate larger aromatics. Analyses were performed online for small aromatics present in higher amounts (e.g. phenol, benzofuran, etc.), whereas offline analyses were performed for heavier aromatics present in lower amounts and therefore demanded a pre-concentration step using the liquid N_2 trapping system. In this system, a Dewar flask was used as it is specialized to hold cryogens like liquid nitrogen. A schematic diagram and the picture of the cold trap assembly used for the sample collection are available in Figure S2 (Supporting Information). The sampling line from the flame was connected to the inlet of a cold borosilicate glass trap which is immersed inside the Dewar flask filled with liquid nitrogen whereas the outlet was connected to a vacuum pump. Apart from withstanding very low temperatures, high quality borosilicate glass has high resistance to chemicals and temperature changes which makes it a suitable candidate for our application. The gaseous sample from the flame passes through the sampling line and consequently flows down the wall of the trap and condenses at the bottom of the trap as liquid nitrogen surrounds the trap. The pressure inside the trap is however constantly regulated (~ 500 torr). After about 40-45 minutes, the cold borosilicate glass trap is disconnected from the sampling system and removed from the Dewar flask. Soon, a little amount of acetone is added to dissolve the condensate in the trap after which the solution was collected in a vial. Next off, this solution was injected using a thin injection syringe (injection volume of 1 µL) and analyzed using the GC-MS systems. Comparison of the chromatograms obtained using freshly prepared samples with those obtained from the same samples after the experiment campaign (a week) indicated no new chemical products, thus ensuring that the chemical makeup of the sample was conserved and no secondary chemical reactions occurred in the vial itself. However, the intensity of the peaks is reduced, indicating that analyte or sample loss occurred over time.

Because of the complexity of the chemical composition of the samples containing OPAHs (and PAHs) from the flame, we thoroughly rechecked the identification using another analytical apparatus. After having analyzed the samples obtained using 1D GC setup in Lille, we set out to perform analysis with the 2D GC-MS (also called "GC×GC") in Ghent by transferring our sample vials in an ice box to transport them. The 2D GC (Thermo Scientific Trace GC Ultra), also equipped with a MS with electron ionization at 70 eV, was used to reevaluate for some species thanks to its enhanced separation mechanism [43]. The same trapped liquid samples were used in both setups. This GC apparatus exploits two different stationary phases in two different columns: a non-polar column (DB-5MS; 30m×0.25mm×0.25µm) and a polar column (DB-17MS; 2m×0.25mm×0.25µm) in the same oven using helium as the carrier gas. A two-jet cryogenic modulator (liquid CO_2) is placed between the two columns and its functions are to trap, isolate, focus and reinject the bands of the eluate from the first column in the second column. The exhaustive transfer of a primary dimension eluting peak into the secondary column could be achieved with an appropriate modulation time (6 seconds in this study). Such a separation mechanism with an enhanced resolution added further information on detection of aromatic species.

3. RESULTS AND DISCUSSION

Mass spectral data can be found in the Excel file provided in the Supporting Information. Section 3.1 presents the obtained 1D GC and 2D GC chromatograms and mass spectra. Section 3.2 details the identified oxygen-containing aromatic substances. In Section 3.3, important experimental indications on the presumed formation kinetics of oxygenated aromatics are discussed. Note that in samples from the flame, in addition to oxygenated aromatics, non-oxygenated aromatics (benzene, naphthalene, phenanthrene, etc.) and other smaller species (CO, CO_2, C_1-C_5 intermediate species, etc.) were also identified. However, the latter species are not presented here as their analysis does not fit with the objective of the present study. Moreover, due to the complexity of this co-existence, the present experiments are limited to three-aromatic-ring species, and the heavier aromatics are the subject of perspective works.

3.1. Overview of the obtained chromatograms and mass spectra

It is worth mentioning that though some exemplary chromatograms at a given flame height are presented in this section to elucidate the primary approach followed for the identification of species, the overall list of identified species is an outcome of the analysis of multiple chromatograms from samples collected at different flame heights. This type of analysis indicated that the signal intensities varied at different HABs confirming their presence at other HABs as well (examples given in the Supporting Information, Figure S3). Furthermore, samples from a flame stabilized at similar conditions containing only iso-octane and methane but no anisole were also collected and analyzed to acknowledge the role of anisole as a doped biofuel on the formation chemistry of oxygenated aromatics. Comparison of the chromatograms showed that none of the oxygenated aromatics were present in measurable amounts in the flame without anisole (examples given in the Supporting Information, Figure S4). Thus, below important examples are presented only for the anisole doped flame.

Figure 2 shows the 1D GC and 2D GC total ion chromatograms of the anisole doped flame at a given HAB and electron impact mass spectra of some selected oxygenated aromatics.

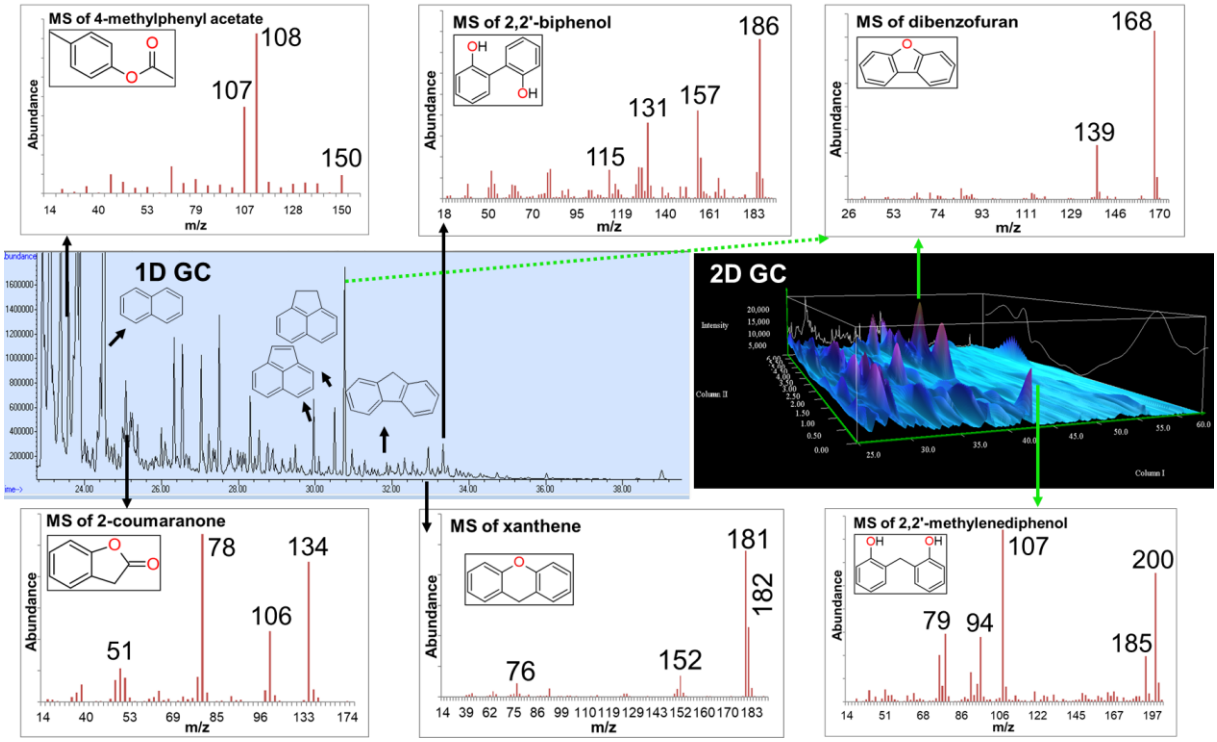

Figure 2. Examples of chromatograms (middle panel) obtained by 1D GC and 2D GC in the anisole doped flame at an HAB=1.5 mm (in the reaction zone). The nomenclature of some important species is given. Some mass spectra (MS, top and bottom panels) for selected oxygenated aromatics obtained by GC-MS systems are presented.

The middle panel of this figure presents two chromatograms obtained via the 1D GC-MS (on the left) and 2D GC-MS (on the right). As described in the experimental section, the columns used for these GC setups (SCION-17MS for 1D GC; DB-5MS and DB-17MS for 2D GC) were specific to aromatic species. Though the chromatogram was very complex and consisted of over 100 peaks, it indicated that several aromatic species are certainly present in the anisole flame. Several peaks amongst these were identified and it was observed that almost 60% of these aromatics were oxygenated, which highlighted their significant co-formation along with classic aromatic species. Following the complexity of the 1D GC chromatogram, we chose to perform additional analyses using the 2D GC-MS as mentioned before. By using

the 2D GC-MS, we could confirm the identification from 1D GC-MS as well as identify additional species besides the ones already identified from 1D GC-MS on account of its different separation mechanism. For example, dibenzofuran ($C_{12}H_8O$) identified by 1D GC-MS was confirmed by 2D GC-MS.

The top and bottom panels of Figure 2 show the mass spectra of these two species and four other selected oxygenated aromatics. The presence of the molecular ion peaks (base peak) and fragment peaks in these spectra are very consistent with the molecular weights and the fragmentation mechanism of the identified molecules.

Figure 3 presents an interested zone of the chromatogram along with selected identified OPAHs and comparisons with pure products. As mentioned earlier, aromatics were identified using both their individual retention times and mass spectrometry spectra. Whenever possible, commercially available pure products were bought to perform direct injections into the GC-MS to confirm their identification, leading to freedom from doubt. Compounds identified by co-injection of commercial standard samples have been indicated in the Excel file for Supporting Information. These pure product injections also allowed us to exclude some isomers. For example, for 2,2′-diphenol and 4-phenoxyphenol (the fourth and the fifth one from left to right in the bottom panel of Figure 3), the peak corresponding to the former species is also present in the flame sample chromatogram, whereas the peak for the latter is not present in the flame sample chromatogram. Thus, the latter was excluded from the list of identified species. When a pure product possessed the same retention time as that of the peak in the flame sample chromatogram (Figure 3) and the MS obtained for the peak in question corresponded well to that proposed from the NIST-MS library [42] or to that of the pure product injection, then the chemical structure of the species was well confirmed without doubt. In case when no pure products were available to reassess the proposition from the GC-MS (based on the NIST library [42] integrated in our GC-MS systems), an analysis of the anticipated fragmentation pattern was performed whenever possible (an example for 4-methylphenyl acetate available in the Supporting Information, Figure S5).

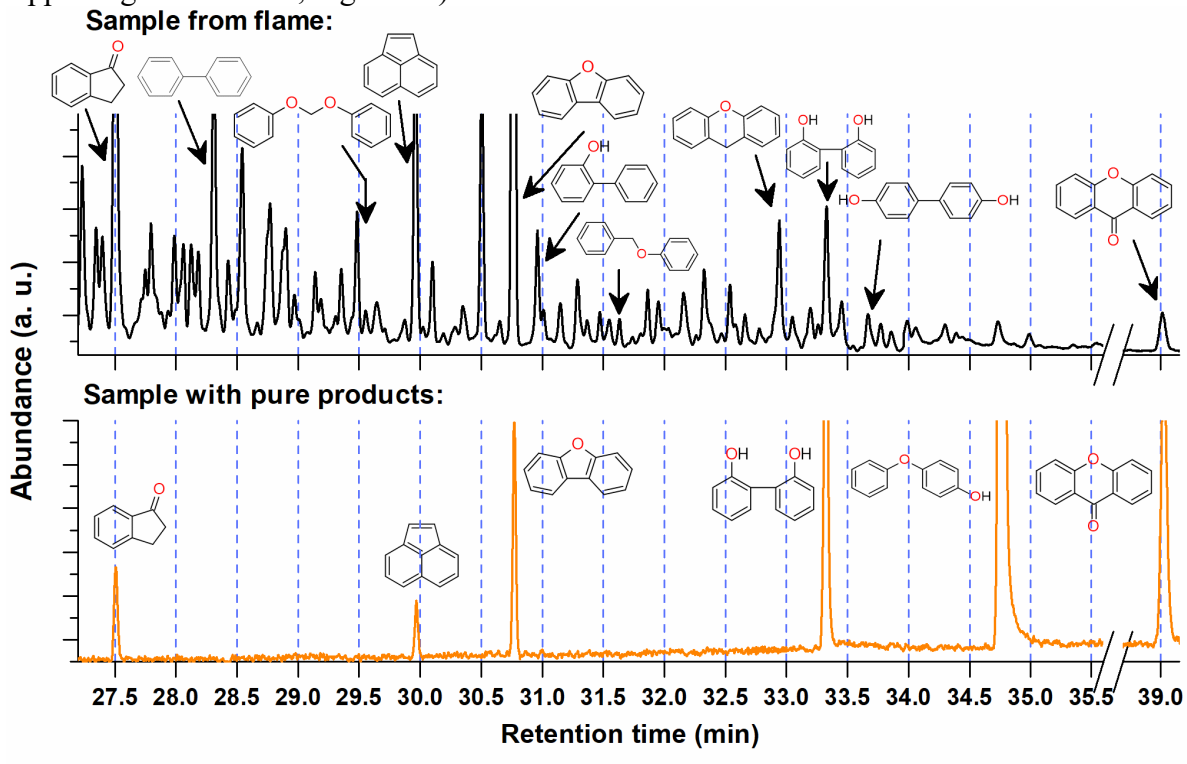

Figure 3. Comparison of a chromatogram obtained from a flame sample (at HAB=1.5 mm) and that from injection of a mixture of known pure products (for clarity only a few examples are presented).

3.2. Identified oxygenated aromatics

Based on the approach described above, approximately 80 oxygenated mono- and polyaromatic compounds were identified. They are reported in Table 1 and Figure 4. While Table 1 presents the different species by mass (with their corresponding chemical formula, common and IUPAC names, and structures respectively), Figure 4 presents a pictorial representation of the identified species in accordance with the number of rings (and similar core structure placed close together) to provide another overview on the detected oxygenated aromatics.

Table 1. Identified oxygenated aromatics in the studied anisole flame together with their names and molar masses (M, g/mol). Detection of these species in literature's experiments is also presented (two columns on the extreme right). The reported data is the result of chromatographic analysis of samples collected at multiple flame heights using variable split ratios of the GC injector. The GC retention time for each species is available in Excel file of the Supporting Information.

Identified in the present flame					**Detected in literature experiments** [b]	
N°	M	Formula	Name [a]	Structure	Flames	Other reactors
1	94	C_6H_6O	*Phenol*	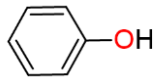	27,33	22,30–32,37,44,45
2	106	C_7H_6O	*Benzaldehyde*	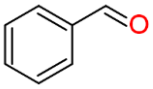	27,33	22,30–32,37,44,46
3	108	C_7H_8O	*Anisole*	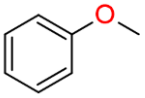	27,33	22,30,31,37,44,46
4	108	C_7H_8O	*o*-Cresol; *2-Methylphenol*	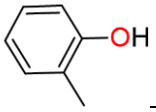	27	21,22,30,32,46
5	108	C_7H_8O	*m*-Cresol; *3-Methylphenol*	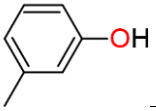		
6	108	C_7H_8O	*p*-Cresol; *4-Methylphenol*	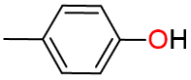	27	21,22,30,32,46
7	110	$C_6H_6O_2$	Hydroquinone; *Benzene-1,4-diol*			
8	118	C_8H_6O	Benzofuran; *1-Benzofuran*	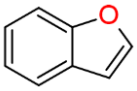	27,33*	21,22,31,32
9	120	C_8H_8O	2,3-Dihydrobenzofuran; *2,3-Dihydro-1-benzofuran*	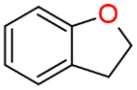		37*
10	122	$C_7H_6O_2$	Salicylaldehyde; *2-Hydroxybenzaldehyde*	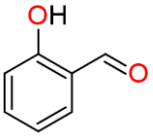		37*; 30**
11	122	$C_7H_6O_2$	*m*-Formylphenol; *3-Hydroxybenzaldehyde*	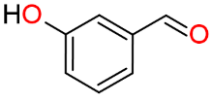		37*; 30**
12	122	$C_7H_6O_2$	*4-Hydroxybenzaldehyde*	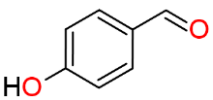		
13	122	$C_7H_6O_2$	1,3-Benzodioxole; *2H-1,3-benzodioxole*	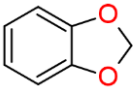		37*

14	122	$C_8H_{10}O$	2,6-Xylenol; *2,6-Dimethylphenol*	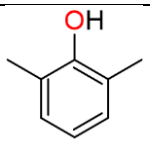		37*
15	122	$C_8H_{10}O$	*2,4-Dimethylphenol*	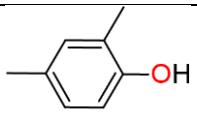		
16	122	$C_8H_{10}O$	*2-Ethyl phenol*	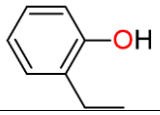	27	31, 37*
17	122	$C_8H_{10}O$	*3-Ethyl phenol*	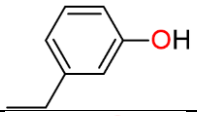		
18	122	$C_8H_{10}O$	Ethyl phenyl ether; *Ethoxybenzene*	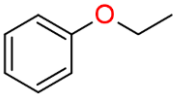		37*
19	122	$C_8H_{10}O$	*1-Methoxy-4-methylbenzene*	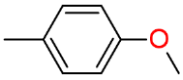		
20	124	$C_7H_8O_2$	*m*-Guaiacol; *3-Methoxyphenol*	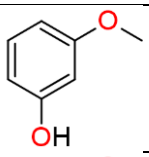		30, 37*
21	124	$C_7H_8O_2$	*o*-Guaiacol; *2-Methoxyphenol*	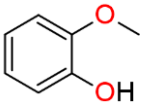	33	
22	124	$C_7H_8O_2$	p-Guaiacol; *4-Methoxyphenol*	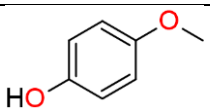		
23	132	C_9H_8O	1-Indanone; *2,3-Dihydro-1H-inden-1-one*	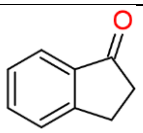		37*
24	132	C_9H_8O	2-Methyl benzofuran; *2-Methyl-1-benzofuran*	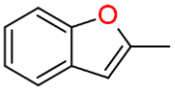		37*
25	132	C_9H_8O	*[(prop-2-yn-1-yl)oxy]benzene*	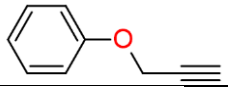		
26	132	C_9H_8O	*1,3-Dihydro-2H-inden-2-one*	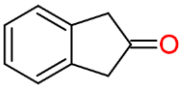		
27	134	$C_8H_6O_2$	2-Coumaranone; *1-Benzofuran-2(3H)-one*	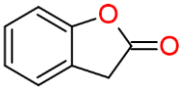		37*
28	134	$C_9H_{10}O$	*[(prop-2-en-1-yl)oxy] benzene*	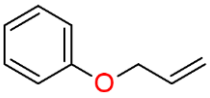		
29	134	$C_9H_{10}O$	*4-(prop-2-en-1-yl) phenol*	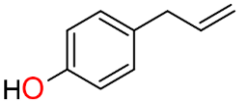		

30	136	$C_8H_8O_2$	*5-Methyl-2H-1,3-benzodioxole*	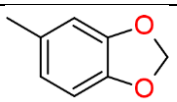	
31	136	$C_8H_8O_2$	*Phenyl acetate*	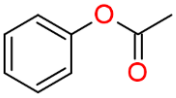	
32	136	$C_9H_{12}O$	5-Ethyl *m*-cresol; *3-Ethyl-5-methylphenol*	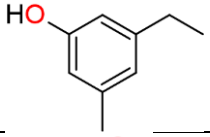	
33	138	$C_8H_{10}O_2$	*3-Methoxy-2-methylphenol*	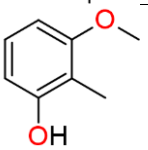	
34	138	$C_8H_{10}O_2$	*3-Ethoxyphenol*	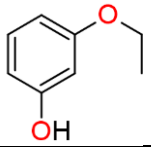	
35	144	$C_{10}H_8O$	2-Vinyl benzofuran; *2-Ethenyl-1-benzofuran*	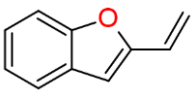	
36	144	$C_{10}H_8O$	1-Naphthol; *Naphthalen-1-ol*	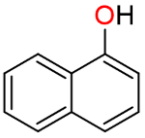	
37	144	$C_{10}H_8O$	2-Naphthol; *Naphthalen-2-ol*	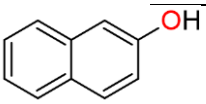	
38	144	$C_{10}H_8O$	3-Phenylfuran	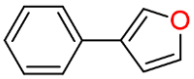	
39	146	$C_{10}H_{10}O$	1-Methylindan-2-one; *1-Methyl-1,3-dihydro-2H-inden-2-one*	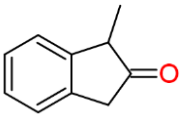	
40	146	$C_{10}H_{10}O$	2-Ethyl benzofuran; *2-Ethyl-1-benzofuran*	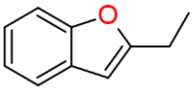	
41	146	$C_{10}H_{10}O$	*1-methyl-4-[(prop-2-yn-1-yl)oxy] benzene*	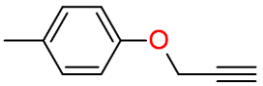	
42	148	$C_{10}H_{12}O$	*2-(2-methylprop-2-en-1-yl) phenol*	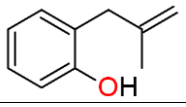	
43	148	$C_{10}H_{12}O$	*4-(2-methylprop-2-en-1-yl) phenol*	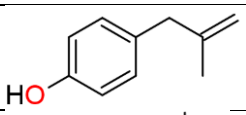	
44	148	$C_{10}H_{12}O$	*[(2-methylprop-2-en-1-yl)oxy] benzene*	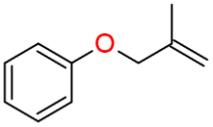	
45	150	$C_9H_{10}O_2$	*p*-Acetoxy toluene;	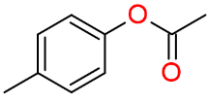	

			4-Methylphenyl acetate			
46	150	$C_9H_{10}O_2$	Phenyl propionate; *Phenyl propanoate*	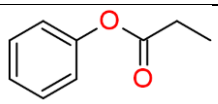		
47	156	$C_{11}H_8O$	2-Naphthaldehyde; *Naphthalene-2-carbaldehyde*	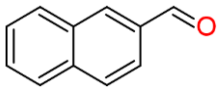		
48	168	$C_{12}H_8O$	Dibenzofuran; *Dibenzo[b,d]furan*	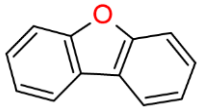	27	30,31,47; 37*
49	168	$C_{12}H_8O$	*Acenaphthylen-1(2H)-one*	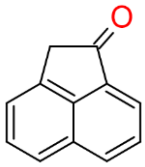		
50	170	$C_{12}H_{10}O$	Diphenyl ether; *1,1'-Oxydibenzene*	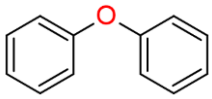		
51	170	$C_{12}H_{10}O$	*o*-Hydroxybiphenyl; *[1,1'-Biphenyl]-2-ol*	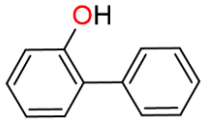		22
52	180	$C_{13}H_8O$	9-Fluorenone; *9H-Fluoren-9-one*	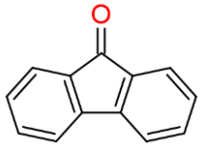		
53	182	$C_{13}H_{10}O$	Xanthene; *9H-Xanthene*	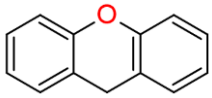		37*
54	182	$C_{13}H_{10}O$	9-Fluorenol; *9H-fluoren-9-ol*	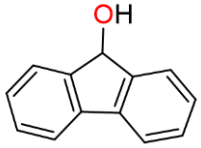		
55	182	$C_{13}H_{10}O$	4-Methyldibenzofuran; *4-Methyldibenzo[b,d]furan*	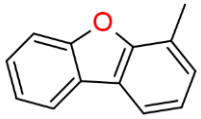		
56	182	$C_{13}H_{10}O$	*6H-Dibenzo[b,d]pyran*	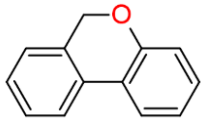		37*
57	184	$C_{12}H_8O_2$	Dibenzo-p-dioxin; *Oxanthrene*	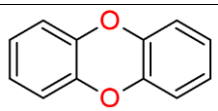		37*
58	184	$C_{12}H_8O_2$	2-Dibenzofuranol; *Dibenzo[b,d]furan-2-ol*	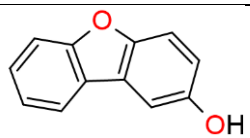		37*
59	184	$C_{13}H_{12}O$	Benzyl phenyl ether; *(Benzyloxy)benzene*	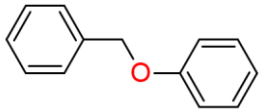		

60	184	$C_{13}H_{12}O$	*o*-Benzylphenol; *2-Benzylphenol*	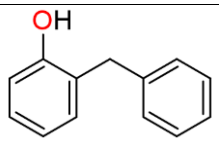	
61	184	$C_{13}H_{12}O$	*p*-Benzylphenol; *4-Benzylphenol*	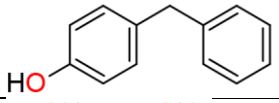	
62	186	$C_{12}H_{10}O_2$	2,2′-Diphenol; *[1,1'-Biphenyl]-2,2'-diol*	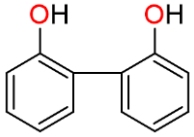	47
63	186	$C_{12}H_{10}O_2$	m-Phenoxy phenol; *3-Phenoxyphenol*	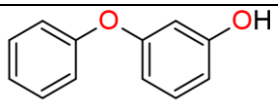	
64	186	$C_{12}H_{10}O_2$	1-Naphthyl acetate; *Naphthalen-1-yl acetate*	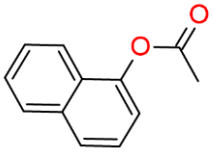	
65	186	$C_{13}H_{14}O$	2-(2-Naphthyl)-2-propanol; *2-(Naphthalen-2-yl)propan-2-ol*	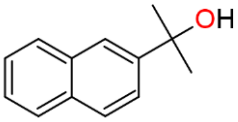	
66	186	$C_{13}H_{14}O$	*2,5,8-Trimethylnaphthalen-1-ol*	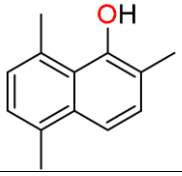	
67	196	$C_{13}H_8O_2$	Xanthone; *9H-Xanthen-9-one*	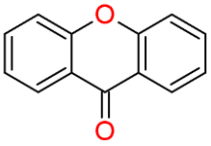	37*
68	200	$C_{13}H_{12}O_2$	Bis (2-hydroxyphenyl) methane; 2,2'-*Methylenediphenol*	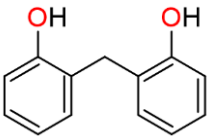	
69	200	$C_{13}H_{12}O_2$	*2-[(4-Hydroxyphenyl)methyl] phenol*	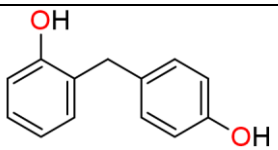	
70	200	$C_{13}H_{12}O_2$	*4,4'-methylenediphenol*	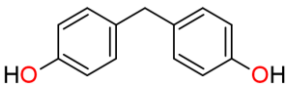	
71	200	$C_{13}H_{12}O_2$	*1,1'-[methylenebis(oxy)] dibenzene*	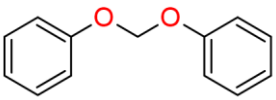	
72	200	$C_{13}H_{12}O_2$	*1-methoxy-2-phenoxybenzene*	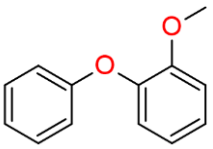	

73	208	$C_{14}H_8O_2$	Anthraquinone; *Anthracene-9,10-dione*	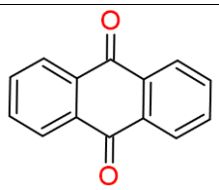	
74	208	$C_{14}H_8O_2$	*Phenanthrene-9,10-dione*	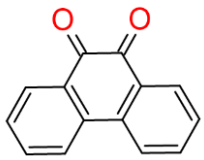	
75	224	$C_{15}H_{12}O_2$	9-Fluorenyl acetate; *9H-Fluoren-9-yl acetate*	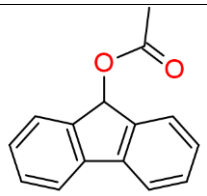	

Table footnotes: [a]: Names in italic refer to the IUPAC nomenclature. [b]: literature studies on anisole as fuel; Here: "*": in the cited reference, the signal corresponding to this mass was detected, but the molecule structure was not experimentally identified (possible isomers were proposed based on theoretical calculations); "**": in the cited reference, hydroxybenzaldehyde is mentioned but not specified which isomer. No listed references indicate that the species were not reported in the literature.

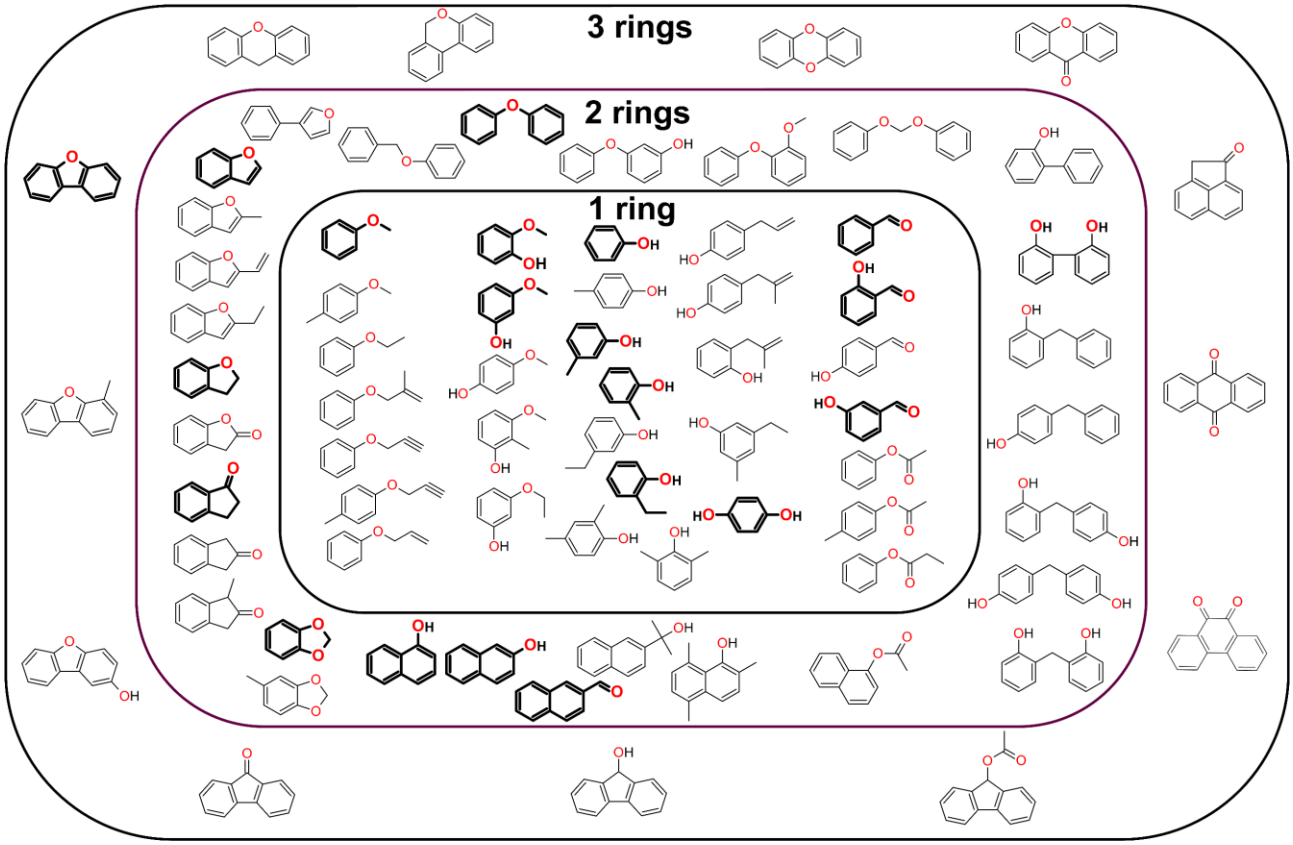

Figure 4. Identified OPAHs in this study with one-, two-, and three-rings, respectively. For each category, somewhat similar core structures are placed in close proximity. Species highlighted in bold font/bonds are those that are already considered in the current kinetic models in the literature (discussed in the following section, Section 3.3).

It is clear that an aromatic ether biofuel like anisole is giving rise to a whole new set of species during its oxidation and decomposition in flames namely OPAHs. The identified oxygenated aromatics have molar masses ranging from 94 (phenol, C_6H_6O) to 224 (9-fluorenyl acetate, $C_{15}H_{12}O_2$) and contain in their structure one or two O-atoms. Though some aromatics containing three or four O-atoms were also proposed by GC-MS by comparing to the NIST-MS database, but since the structure of these molecules is even more complex we prefer not to solely rely on the numerical values for the match factors and in fact find pure analytes in order to confirm their identification in the future. Therefore, such species have not been presented in this paper. Amongst the species listed previously, we distinguished and identified several different isomers such as C_7H_8O (mass 108, 4 isomers), $C_{10}H_8O$ (mass 144, 4 isomers), $C_{13}H_{10}O$ (mass 182, 4 isomers). Also, species with same molar masses (isomeric or non-isomeric) could also be well distinguished and identified, such as 10 species at mass 122, 5 species at mass 184, 5 species at mass 186 and so on. Some species, for instance, 4-methyldibenzo[b,d]furan ($C_{13}H_{10}O$, mass 182, N°55) and 2,5,8-trimethylnaphthalen-1-ol ($C_{13}H_{14}O$; mass 186, N°66) were observed only using 2D GC-MS. Separating and identifying such complex compositions is already considered to be very challenging for different techniques [31,33,37]. Compared to the literature, more than half of the species detected in our study are reported for the first time for anisole combustion (see Table 1; last two columns on the right). Concretely, amongst the 75 oxygenated aromatics listed in Table 1, 67 species (~90%) are reported for the first time as compared to the literature studies under flame conditions, and 51-65 species (~67-86%, depending on whether Ref [37] is taken into account or not) are reported for the first time with experimental evidence as compared to the literature studies in other reactors. As presented in Table 1, a significant percentage (~50%) of oxygenated one-ring aromatics were also reported by the literature studies, while this percentage is around ~30% and ~10% for two-ring and three-ring oxygenated aromatics, respectively.

It is worth mentioning that despite the potential of our GC systems, we still encountered some difficulties in the separation of some species. Concretely, some species can be identified, but their peaks are in the vicinity of other neighboring intense peaks which leads to difficulties in peak integration process. For instance, amongst the three guaiacols (mass 124), peaks for o- and p-guaiacol were right before the intense peak of m-guaiacol which made it really difficult to distinguish between o- and p-guaiacols. Similarly, because of their close retention times, it was very challenging to separate 2-methoxyphenol from 4-methoxyphenol ($C_7H_8O_2$), naphthalen-1-ol from naphthalen-2-ol ($C_{10}H_8O$), 2-benzylphenol from 4-benzylphenol ($C_{13}H_{12}O$), and bis (2-hydroxyphenyl) methane (2,2'-methylenediphenol) from 2-[(4-hydroxyphenyl) methyl] phenol ($C_{13}H_{12}O_2$). However, 2-benzylphenol and 4-benzylphenol ($C_{13}H_{12}O$), bis (2-hydroxyphenyl) methane (2,2'-methylenediphenol) and 2-[(4-hydroxyphenyl) methyl] phenol ($C_{13}H_{12}O_2$) were well separated in the 2D GC-MS chromatogram. In addition, there were about 13 intense peaks which could not be identified using our MS systems. The dissociation/fragmentation patterns corresponding to these signals were not distinct and could not be recognized. Hence, as per the NIST-MS database several matches/possibilities with very low probabilities for the match were proposed. In some other cases, isomers could not be distinguished as the dissociation/fragmentation patterns were similar and sometimes the proposed matches were not even close to the structures anticipated. Since the analytical standards for some species of interest do not exist, their identification is ambiguous as there is no reference for comparison in the NIST database.

Table 1 and Figure 4 show that the detected oxygenated aromatics possess different functionalities such as: alcohol, ether, carbonyl (aldehyde and ketone), and ester. The number of aromatics belonging to a particular functional group were counted and are summarized in Figure 5. Alcohols and ethers are predominant (35 and 32 species, respectively) functionalities amongst these species. The abundance of ethers could perhaps be related to the structure of anisole i.e., an aromatic ether. But interestingly, 15 out of 32 ethers are cyclic ethers (O atom in the cycle) whereas anisole itself is not a cyclic ether which indicates the existence of different mechanisms for the formation of ethers from anisole. Some of these possibilities are described in the next section. The abundance of alcohols (35

species) underlines that the conversion of the aromatic ether as a fuel to alcoholic products is an important process under the studied conditions.

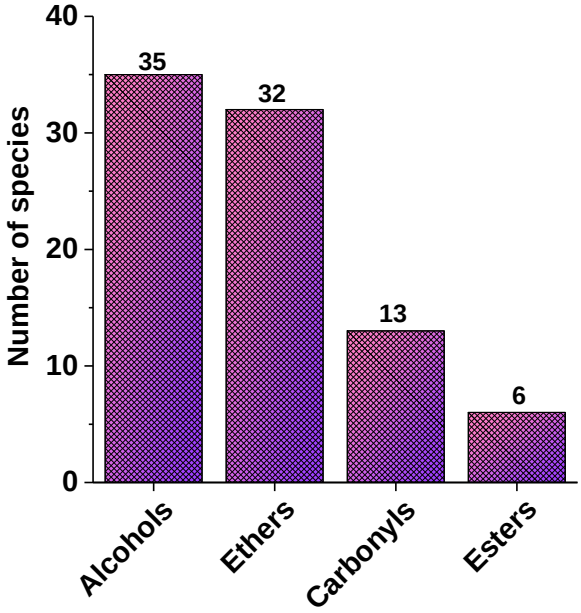

Figure 5. Number of oxygenated aromatics with different functional groups. Carbonyls include aldehydes and ketones. Species containing two identical functional groups is counted once, e.g. dibenzo-p-dioxin ($C_{12}H_8O_2$) with two ether groups. Some species were counted twice if they contained two different functional groups, e.g. 2-dibenzofuranol consists of an ether and an alcohol functional group and so is counted twice. Thus, the total number presented is greater than that for Table 1.

3.3. Experimental indications of the formation kinetics of oxygenated aromatics

Different models were developed for the pyrolysis and combustion of anisole in the literature, such as Roy and Askari model in 2022 [48], Chen et al. model in 2022 [27], Mergulhão et al. model in 2021 [26], Büttgen et al. model in 2020 [25], CRECK model in 2020 [49] , Yuan et al. model in 2019 [31], Wagnon et al. model in 2018 [21], Nowakowska et al. model in 2014 [30]. Some of these models include oxygenated aromatics [27,30,31,49]. In Figure 4, the species highlighted by bold font/bonds were the ones that are considered in the models in the literature. Eleven one-ring and eight two-ring oxygenated aromatics have been considered in the literature models [27,30,31,49]. However, only one out of thirteen three-ring species is considered in these models (Figure 4). The detection of oxygenated aromatics in the present study thus opens an important perspective for the combustion community for the further development of kinetic models for this lignin-based biofuel. Based on the discussion of chemical pathways leading to the formation of relevant oxygenated aromatics from the literature and our experimental identifications, we present a pictorial representation of these pathways for certain relevant oxygenated aromatics from anisole in Figure 6.

As mentioned previously, aromatics with the alcohol functional group were the most abundant amongst the identified species. This indicates that addition of the OH radicals on the double bonds of the benzene ring (from anisole or subsequent products) followed by the subsequent C–H or C–C β-scissions could be one of the possible mechanisms contributing to the formation of these species. Figure 6 presents examples of this mechanism for the formation of o-guaiacol and phenol from anisole. The formation of the two latter species via this mechanism was also presented in Ref [33]. The formation of larger phenols from larger aromatic products via this mechanism could be also expected. A second possible mechanism leading to the formation of alcoholic aromatics is the tautomerization of aromatic ketones to aromatic alcohols, where the ketones could be produced from the combination of the phenoxy (C_6H_5O) radical with other aromatic radicals. Figure 6 presents examples of this mechanism for the formation of 2,2′-diphenol and o-benzylphenol.

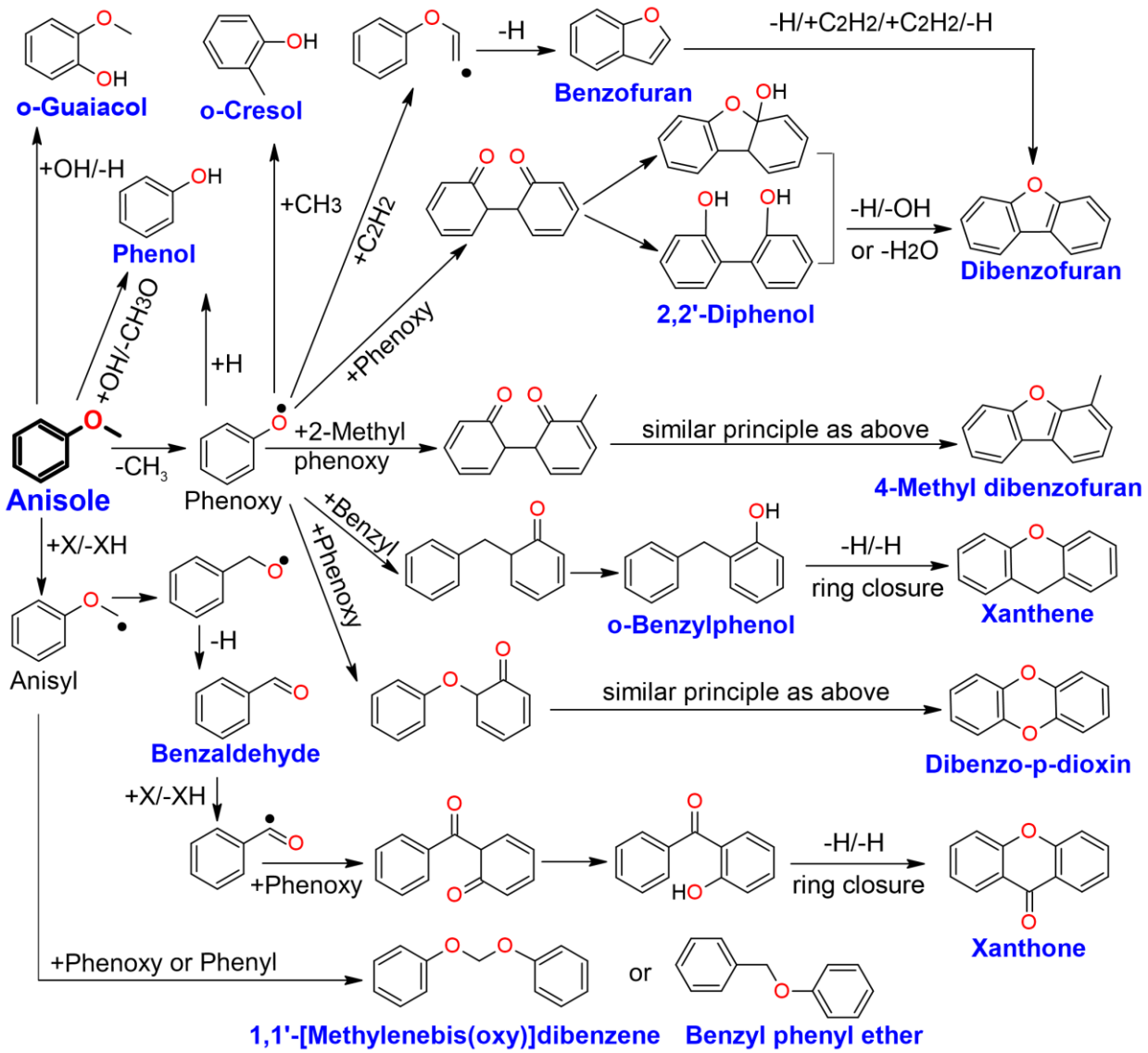

Figure 6. Some possible formation routes leading to the formation of some relevant oxygenated aromatics. Stable species with their names were experimentally identified in the present work.

The O-CH_3 bond in the methoxy group of anisole has a very low bond dissociation energy (63.2 kcal/mol), owing to which its unimolecular O-C bond cleavage to yield phenoxy (C_6H_5O) and methyl (CH_3) radicals is strongly favored, especially under fuel-rich conditions [33]. Phenoxy is a resonance stabilized radical, that may react to form different oxygenated aromatics. For instance, they could recombine with H atoms to contribute to the formation of phenol, react with the CH_3 radical to form o-cresol [30] and with C_2H_2 to form benzofuran [31,50] that may enlarge via H-abstraction and C_2H_2 addition reactions to produce dibenzofuran (a three-ring OPAH) [50]. The phenoxy radicals themselves may also undergo self-recombination reactions followed by subsequent intramolecular rearrangements which may adequately elucidate the formation pathway to produce dibenzofuran [31,51]. 2,2'-Diphenol, an intermediate species in this pathway, was experimentally identified in the present work. A similar principle can be applied for the formation of 4-methyl dibenzofuran, but from the recombination of phenoxy and 2-methyl phenoxy radicals. The self-recombination of the phenoxy radical and its combination with the benzyl radical can lead to the formation of dibenzo-p-dioxin and xanthene, respectively. While the formation of dibenzo-p-dioxin via this pathway was investigated in the literature [51], the formation of xanthene via this way is suggested by the detection of o-benzylphenol in the present work.

Anisole itself may undergo H-atom abstraction on the methoxy group in order to yield the anisyl ($C_6H_5OCH_2$) radical. This anisyl radical can isomerize to the benzoxyl ($C_6H_5CH_2O$) radical via the

ipso-rearrangement, followed by a β-scission reaction to yield benzaldehyde [30]. The experimental detection of xanthone suggests a possible involvement of benzaldehyde in the formation of OPAHs through the recombination of its radical with other aromatic radicals such as phenoxy. Furthermore, the detection of 1,1'-[methylenebis(oxy)]dibenzene and benzyl phenyl ether could be envisaged at the recombination of anisyl radical with the phenoxy and phenyl radicals, respectively. Future studies focusing on the comprehensive development of a kinetic model for anisole could include and test these suggested formation pathways.

It must be noted that the reaction pathways for OPAHs cited in the previous paragraphs are limited to anisole as their precursor. However, other formation routes cannot be excluded, e.g. pathways involving PAHs, because the formation of OPAHs from classical PAHs could also be relevant. For example, the formation of dibenzofuran from biphenyl could also be possible[50,52]. However, this contribution could be less significant as compared to the direct formation pathways via anisole as none of the OPAHs were observed in detectable amounts in another flame that we studied without anisole addition (refer to the Supporting Information, Figure S4, for details). Thus, straight-thinking implies that the formation of OPAHs detected in the anisole doped flame is mainly controlled by the presence of anisole. Nevertheless, there could be some oxygenated aromatics that could be formed because of interaction between the chemistry of anisole and iso-octane. The experimentally-detected species indicated this possibility that is exemplarily summarized in a schematic representation in Figure 7. For instance, iso-octane can undergo H-abstraction to produce iso-octyl radicals. Depending on the site of H-abstraction, these radicals could further decompose and lead to the formation of propenyl and isobutenyl radicals. These radicals could intervene with the consumption steps of phenoxy radicals. For example, the isobutenyl radical could attack either on the oxygen atom or the ortho position or the para position of the phenoxy radical followed by isomerization to produce [(2-methylprop-2-en-1-yl)oxy] benzene, 2-(2-methylprop-2-en-1-yl) phenol, and 4-(2-methylprop-2-en-1-yl) phenol. All these oxygenated aromatics were detected in the present experiment (Table 1), which could evidence this mechanism. Similarly, the propenyl radical could attack the phenoxy radical to produce [(prop-2-en-1-yl)oxy] benzene, 2-(prop-2-en-1-yl) phenol, and 4-(prop-2-en-1-yl) phenol, respectively. The former and the latter were experimentally observed in this study (Table 1). Furthermore, the detection of 1-methyl-4-[(prop-2-yn-1-yl)oxy] benzene confirms the participation of C_1 and C_2 species. The ipso-addition of CH_3 (a radical produced by the three fuels) on anisole leads to the formation of 1-methoxy-4-methylbenzene (also experimentally detected) that can react to yield 1-methyl-4-[(prop-2-yn-1-yl)oxy] benzene via H-abstraction and C_2H_2 recombination. C_2H_2 here could be produced from either of the three fuels in the mixture via different pathways. It must be noted that the reactions proposed do not constitute a complete mechanism but are mere possibilities based on the qualitative analysis of the species that were experimentally identified in this work. More species and more pathways could certainly exist. A quantitative evaluation of the contribution of iso-octane/methane was not performed in the current work as it does not align with the objective of this work i.e., experimental evidence-based identification of oxygenated aromatics in an anisole doped flame. But it is an interesting subject for the future work. Note that we also changed the equivalence ratio (between 1.72-1.90) and the amount of the added anisole (between 5%-15%). The resulting GC-MS data showed that the signal intensity of peaks in chromatograms changed, while the identification of oxygenated aromatics was the same.

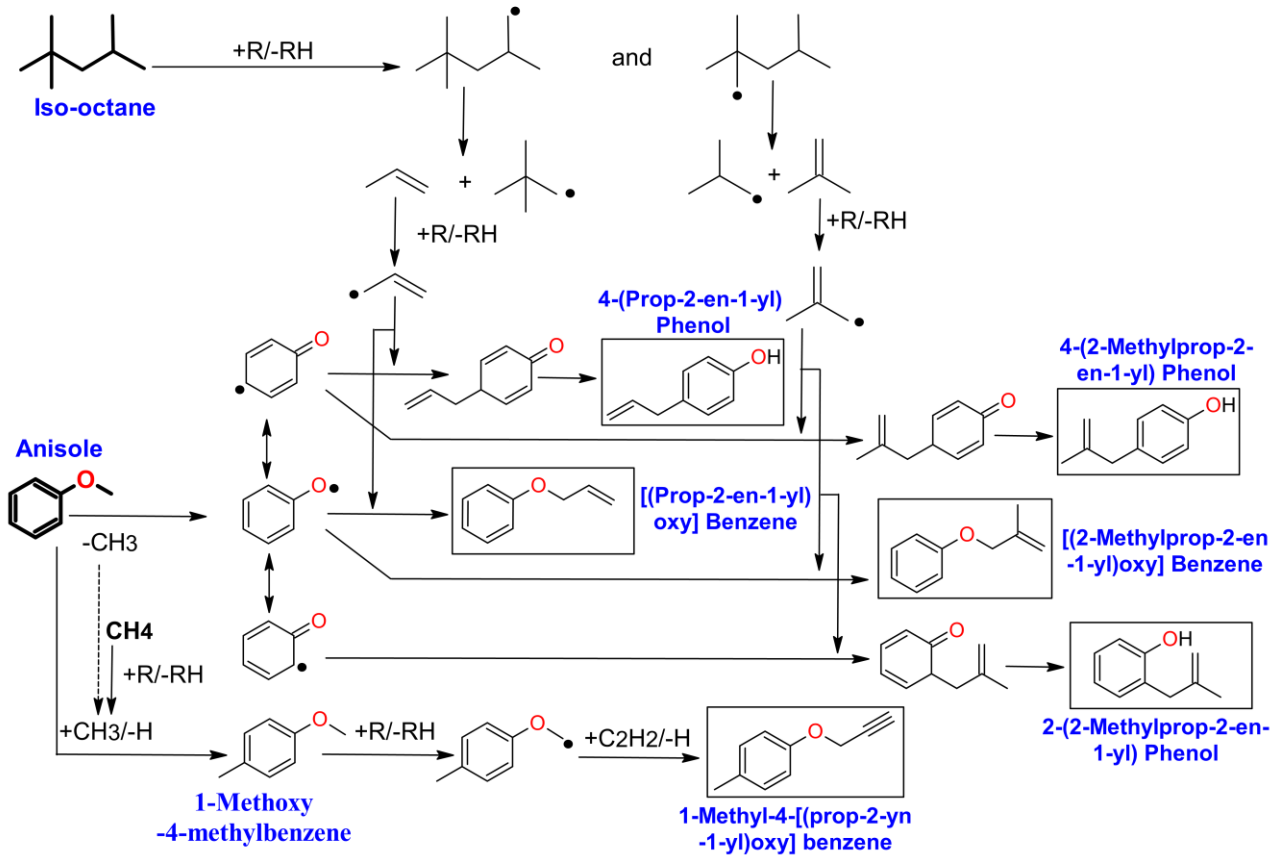

Figure 7. Some possible formation routes leading to the formation of some other relevant oxygenated aromatics considering the smaller species formed via iso-octane. Stable species with their names were experimentally identified in the present work. Species enclosed in rectangles are involved in discussions of iso-octane/methane contribution. Here R: H, OH, etc.

4. CONCLUSION AND PERSPECTIVES

The aromatic ring in anisole in combination with the methoxy group makes it the simplest model compound for lignin-based biofuels. The experimental detection of oxygenated aromatics from a laminar atmospheric fuel-rich anisole doped premixed flames is performed by using 1D and 2D GC-MS systems. About 80 oxygenated aromatics have been identified in this work. About 90% species are reported for the first time as compared to the literature studies under flame conditions, and about 70% of species are reported for the first time as compared to the literature studies in other miscellaneous reactors. While ~50% of the oxygenated one-ring aromatics detected in the present study were also reported by the literature studies, this percentage is more limited, only ~30% and ~10%, for two-ring and three-ring oxygenated aromatics, respectively. The detected oxygenated aromatics possess different functionalities such as: alcohol, ether, carbonyl (aldehyde and ketone), and ester, with alcohols and ethers being more predominant. The large number of detected alcohols underlines the important conversion mechanism of anisole to alcoholic products. Furthermore, ~50% of the ethers detected are cyclic ethers (O atom in the ring) whereas anisole itself is not a cyclic ether, implying that among the decomposition pathways considered, the ring-closing reaction followed by C-H or O-H β-scission reactions are predominant in the formation of these types of OPAHs from anisole. In addition, the newly detected species highlight that not only phenoxy radicals (produced by cleavage of the O-CH_3 bond of anisole) but also the anisyl radical (formed by H-abstractions on the CH_3 of anisole) plays an important role in the formation of OPAHs. Some possible formation pathways of experimentally identified oxygenated aromatics are presented and discussed.

The identification now allows us to move to next step: quantification of these species and study of their relationship with classical PAHs and with soot formation, which is currently an ongoing project

at our team. As mentioned earlier, qualitative analysis shows that the number of alcoholic aromatics were more abundant in comparison to other oxygenated functionalities. However, it could be possible that the latter are present in greater amounts than the former. This could imply that though the alcohol functional group is the most frequently encountered functional group amongst the list of identified oxygenated aromatics qualitatively, their quantification would reveal whether they are the most abundant functional group quantitatively as well. Note that these tasks are again very challenging because of their state (solid phase at room temperature). Moreover, identification of OPAHs containing from 3 O-atoms and 4-ring aromatics is also envisaged. Because of their great complexity, supplemental techniques based on other detection principles would be necessary, for instance, the synchrotron-based photoelectron photo ion coincidence (SVUV-PEPICO) spectroscopy at the SOLEIL synchrotron, inspired from our recent measurement campaigns for complex oxygenated components [53].

ACKNOWLEDGEMENTS

The authors would like to thank ADEME (The French Agency for the Ecological Transition) and the Hauts-de-France Region for their financial support. The work was funded by the support from I-SITE via the Biofuel-Soot project (R-JEUNES CHERCHEURS-19-010-TRAN). The support from IREPSE (L'Institut de Recherches Pluridisciplinaires en Sciences de l'Environnement) is also appreciated. The work was further supported by the French Ministère de l'Europe et des Affaires Étrangères, the French Ministère de l'Enseignement Supérieur et de la Recherche, and the European Funds for Regional Economic Development for their financial support via the PHC Alliance 2022 programme (project No: 47860XL) and via the CPER research project CLIMIBIO, respectively. The authors would like to thank Léo Delcambre for his contribution to pure OPAH analyses.

ASSOCIATED CONTENT

Supporting Information:

Two Supporting Information files available:

1/ Pictures and schematic representation for flame burner, fuel system, and cold trap (PDF)

2/ Mass spectra of identified oxygenated aromatics (Excel)

REFERENCES

(1) IEA. World Energy Outlook 2022. IEA, Paris Https://Www.Iea.Org/Reports/World-Energy-Outlook-2022, License: CC BY 4.0 (Report); CC BY NC SA 4.0 (Annex A); 2022. https://www.iea.org/topics/world-energy-outlook (accessed 2022-11-07).

(2) Leitner, W.; Klankermayer, J.; Pischinger, S.; Pitsch, H.; Kohse-Höinghaus, K. Advanced Biofuels and beyond: Chemistry Solutions for Propulsion and Production. Angew. Chem. - Int. Ed. **2017**, 56 (20), 5412–5452. https://doi.org/10.1002/anie.201607257.

(3) Tran, L.-S.; Herbinet, O.; Carstensen, H.-H.; Battin-Leclerc, F. Chemical Kinetics of Cyclic Ethers in Combustion. Prog. Energy Combust. Sci. **2022**, 92, 101019. https://doi.org/10.1016/j.pecs.2022.101019.

(4) Ma, J.; Shi, S.; Jia, X.; Xia, F.; Ma, H.; Gao, J.; Xu, J. Advances in Catalytic Conversion of Lignocellulose to Chemicals and Liquid Fuels. J. Energy Chem. **2019**, 36, 74–86. https://doi.org/10.1016/j.jechem.2019.04.026.

(5) Bonawitz, N. D.; Chapple, C. The Genetics of Lignin Biosynthesis: Connecting Genotype to Phenotype. Annu. Rev. Genet. **2010**, 44, 337–363. https://doi.org/10.1146/annurev-genet-102209-163508.

(6) Wang, M.; Ma, J.; Liu, H.; Luo, N.; Zhao, Z.; Wang, F. Sustainable Productions of Organic Acids and Their Derivatives from Biomass via Selective Oxidative Cleavage of C–C Bond. ACS Catal. **2018**, 8 (3), 2129–2165. https://doi.org/10.1021/acscatal.7b03790.

(7) Chiaramonti, D.; Buffi, M.; Palmisano, P.; Redaelli, S. Lignin-Based Advanced Biofuels: A Novel Route towards Aviation Fuels. Chem. Eng. Trans. **2016**, 50, 109–114. https://doi.org/10.3303/CET1650019.
(8) Cotana, F.; Cavalaglio, G.; Nicolini, A.; Gelosia, M.; Coccia, V.; Petrozzi, A.; Brinchi, L. Lignin as Co-Product of Second Generation Bioethanol Production from Ligno-Cellulosic Biomass. Energy Procedia **2014**, 45, 52–60. https://doi.org/10.1016/j.egypro.2014.01.007.
(9) Kim, Y.; Etz, B. D.; Fioroni, G. M.; Hays, C. K.; St. John, P. C.; Messerly, R. A.; Vyas, S.; Beekley, B. P.; Guo, F.; McEnally, et al. Investigation of Structural Effects of Aromatic Compounds on Sooting Tendency with Mechanistic Insight into Ethylphenol Isomers. Proc. Combust. Inst. **2021**, 38 (1), 1143–1151. https://doi.org/10.1016/j.proci.2020.06.321.
(10) Guan, C.; Cheung, C. S.; Li, X.; Huang, Z. Effects of Oxygenated Fuels on the Particle-Phase Compounds Emitted from a Diesel Engine. Atmospheric Pollut. Res. **2017**, 8 (2), 209–220. https://doi.org/10.1016/j.apr.2016.08.005.
(11) Xu, L.; Wang, Y.; Liu, D. Effects of Oxygenated Biofuel Additives on Soot Formation: A Comprehensive Review of Laboratory-Scale Studies. Fuel **2022**, 313, 122635. https://doi.org/10.1016/j.fuel.2021.122635.
(12) Lundstedt, S.; White, P. A.; Lemieux, C. L.; Lynes, K. D.; Lambert, I. B.; Öberg, L.; Haglund, P.; Tysklind, M. Sources, Fate, and Toxic Hazards of Oxygenated Polycyclic Aromatic Hydrocarbons (PAHs) at PAH- Contaminated Sites. AMBIO J. Hum. Environ. **2007**, 36 (6), 475–485. https://doi.org/10.1579/0044-7447(2007)36[475:SFATHO]2.0.CO;2.
(13) Lampi, M. A.; Gurska, J.; McDonald, K. I. C.; Xie, F.; Huang, X.-D.; Dixon, D. G.; Greenberg, B. M. Photoinduced Toxicity of Polycyclic Aromatic Hydrocarbons to Daphnia Magna: Ultraviolet-Mediated Effects and the Toxicity of Polycyclic Aromatic Hydrocarbon Photoproducts. Environ. Toxicol. Chem. **2006**, 25 (4), 1079–1087. https://doi.org/10.1897/05-276r.1.
(14) Yu, H. Environmental Carcinogenic Polycyclic Aromatic Hydrocarbons: Photochemistry And Phototoxicity. J. Environ. Sci. Health Part C Environ. Carcinog. Ecotoxicol. Rev. **2002**, 20 (2), 10.1081/GNC-120016203. https://doi.org/10.1081/GNC-120016203.
(15) Walgraeve, C.; Demeestere, K.; Dewulf, J.; Zimmermann, R.; Van Langenhove, H. Oxygenated Polycyclic Aromatic Hydrocarbons in Atmospheric Particulate Matter: Molecular Characterization and Occurrence. Atmos. Environ. **2010**, 44 (15), 1831–1846. https://doi.org/10.1016/j.atmosenv.2009.12.004.
(16) Hartnik, T.; Norli, H. R.; Eggen, T.; Breedveld, G. D. Bioassay-Directed Identification of Toxic Organic Compounds in Creosote-Contaminated Groundwater. Chemosphere **2007**, 66 (3), 435–443. https://doi.org/10.1016/j.chemosphere.2006.06.031.
(17) Bamforth, S. M.; Singleton, I. Bioremediation of Polycyclic Aromatic Hydrocarbons: Current Knowledge and Future Directions. J. Chem. Technol. Biotechnol. **2005**, 80 (7), 723–736. https://doi.org/10.1002/jctb.1276.
(18) Kochany, J.; Maguire, R. J. Abiotic Transformations of Polynuclear Aromatic Hydrocarbons and Polynuclear Aromatic Nitrogen Heterocycles in Aquatic Environments. Sci. Total Environ. **1994**, 144 (1), 17–31. https://doi.org/10.1016/0048-9697(94)90424-3.
(19) Cerniglia, C. E. Fungal Metabolism of Polycyclic Aromatic Hydrocarbons: Past, Present and Future Applications in Bioremediation. J. Ind. Microbiol. Biotechnol. **1997**, 19 (5–6), 324–333. https://doi.org/10.1038/sj.jim.2900459.
(20) Battin-Leclerc, F.; Delort, N.; Meziane, I.; Herbinet, O.; Sang, Y.; Li, Y. Possible Use as Biofuels of Monoaromatic Oxygenates Produced by Lignin Catalytic Conversion: A Review. Catal. Today **2023**, 408, 150–167. https://doi.org/10.1016/j.cattod.2022.06.006.
(21) Wagnon, S. W.; Thion, S.; Nilsson, E. J. K.; Mehl, M.; Serinyel, Z.; Zhang, K.; Dagaut, P.; Konnov, A. A.; Dayma, G.; Pitz, W. J. Experimental and Modeling Studies of a Biofuel Surrogate Compound: Laminar Burning Velocities and Jet-Stirred Reactor Measurements of Anisole. Combust. Flame **2018**, 189, 325–336. https://doi.org/10.1016/j.combustflame.2017.10.020.

(22) Pelucchi, M.; Faravelli, T.; Frassoldati, A.; Ranzi, E.; SriBala, G.; Marin, G.; Geem, K. V. Experimental and Kinetic Modeling Study of Pyrolysis and Combustion of Anisole. Chem. Eng. Trans. **2018**, 65, 127–132. https://doi.org/10.3303/CET1865022.
(23) Zhou, L.; Boot, M. D.; De Goey, L. P. H. Gasoline - Ignition Improver - Oxygenate Blends as Fuels for Advanced Compression Ignition Combustion. SAE Tech. Pap. **2013**, 2. https://doi.org/10.4271/2013-01-0529.
(24) Herzler, J.; Fikri, M.; Schulz, C. Ignition Delay Time Study of Aromatic LIF Tracers in a Wide Temperature and Pressure Range; Boston MA, 2017.
(25) Büttgen, R. D.; Tian, M.; Fenard, Y.; Minwegen, H.; Boot, M. D.; Heufer, K. A. An Experimental, Theoretical and Kinetic Modelling Study on the Reactivity of a Lignin Model Compound Anisole under Engine-Relevant Conditions. Fuel **2020**, 269, 117190. https://doi.org/10.1016/j.fuel.2020.117190.
(26) Mergulhão, C. S.; Carstensen, H.-H.; Song, H.; Wagnon, S. W.; Pitz, W. J.; Vanhove, G. Probing the Antiknock Effect of Anisole through an Ignition, Speciation and Modeling Study of Its Blends with Isooctane. Proc. Combust. Inst. **2021**, 38 (1), 739–748. https://doi.org/10.1016/j.proci.2020.08.013.
(27) Chen, B.; Hellmuth, M.; Faller, S.; May, L.; Liu, P.; Cai, L.; Roberts, W. L.; Pitsch, H. Exploring the Combustion Chemistry of Anisole in Laminar Counterflow Diffusion-Flames under Oxy-Fuel Conditions. Combust. Flame **2022**, 243, 111929. https://doi.org/10.1016/j.combustflame.2021.111929.
(28) Zare, S.; Roy, S.; El Maadi, A.; Askari, O. An Investigation on Laminar Burning Speed and Flame Structure of Anisole-Air Mixture. Fuel **2019**, 244, 120–131. https://doi.org/10.1016/j.fuel.2019.01.149.
(29) Zabeti, S.; Aghsaee, M.; Fikri, M.; Welz, O.; Schulz, C. Optical Properties and Pyrolysis of Shock-Heated Gas-Phase Anisole. Proc. Combust. Inst. **2017**, 36 (3), 4525–4532. https://doi.org/10.1016/j.proci.2016.06.156.
(30) Nowakowska, M.; Herbinet, O.; Dufour, A.; Glaude, P.-A. Detailed Kinetic Study of Anisole Pyrolysis and Oxidation to Understand Tar Formation during Biomass Combustion and Gasification. Combust. Flame **2014**, 161 (6), 1474–1488. https://doi.org/10.1016/j.combustflame.2013.11.024.
(31) Yuan, W.; Li, T.; Li, Y.; Zeng, M.; Zhang, Y.; Zou, J.; Cao, C.; Li, W.; Yang, J.; Qi, F. Experimental and Kinetic Modeling Investigation on Anisole Pyrolysis: Implications on Phenoxy and Cyclopentadienyl Chemistry. Combust. Flame **2019**, 201, 187–199. https://doi.org/10.1016/j.combustflame.2018.12.028.
(32) Zhang, T.; Bhattarai, C.; Son, Y.; Samburova, V.; Khlystov, A.; Varganov, S. A. Reaction Mechanisms of Anisole Pyrolysis at Different Temperatures: Experimental and Theoretical Studies. Energy Fuels **2021**, 35 (12), 9994–10008. https://doi.org/10.1021/acs.energyfuels.1c00858.
(33) Bierkandt, T.; Hemberger, P.; Oßwald, P.; Krüger, D.; Köhler, M.; Kasper, T. Flame Structure of Laminar Premixed Anisole Flames Investigated by Photoionization Mass Spectrometry and Photoelectron Spectroscopy. Proc. Combust. Inst. **2019**, 37 (2), 1579–1587. https://doi.org/10.1016/j.proci.2018.07.037.
(34) Cruz, J. J.; Escudero, F.; Verdugo, I.; Rivera, P.; Gutiérrez-Cáceres, N.; Yon, J.; Fuentes, A. Sooting Propensity and Maturity of Gasoline/Anisole Blends in a Laminar Coflow Diffusion Flame. Fuel **2023**, 345, 128091. https://doi.org/10.1016/j.fuel.2023.128091.
(35) Xiong, G.; Xie, J.; Chen, L.; Wang, W.; Zhou, L. Sooting Tendency of N-Heptane/Anisole Blends in Laminar Counter-Flow Flames with Oxygen Enrichment. Fuel **2019**, 255, 115820. https://doi.org/10.1016/j.fuel.2019.115820.
(36) Zhang, C.; Wu, Y.; Liu, B.; Wang, Z.; Zhou, L. Investigation of Soot Particles Morphology and Size Distribution Produced in a N-Heptane/Anisole Laminar Diffusion Flame Based on TEM Images. Combust. Flame **2022**, 244, 112234. https://doi.org/10.1016/j.combustflame.2022.112234.

(37) Chen, B.; Kruse, S.; Schmid, R.; Cai, L.; Hansen, N.; Pitsch, H. Oxygenated PAH Formation Chemistry Investigation in Anisole Jet Stirred Reactor Oxidation by a Thermodynamic Approach. Energy Fuels **2021**, 35 (2), 1535–1545. https://doi.org/10.1021/acs.energyfuels.0c03829.
(38) Kumar, R.; Kumar, S. Formulation of a Three-Component Gasoline Surrogate Model Using Laminar Burning Velocity Data at Elevated Mixture Temperatures. Fuel **2021**, 306, 121581. https://doi.org/10.1016/j.fuel.2021.121581.
(39) Kalvakala, K. C.; Pal, P.; Kukkadapu, G.; McNenly, M.; Aggarwal, S. Numerical Study of PAHs and Soot Emissions from Gasoline–Methanol, Gasoline–Ethanol, and Gasoline–n-Butanol Blend Surrogates. Energy Fuels **2022**, 36 (13), 7052–7064. https://doi.org/10.1021/acs.energyfuels.2c00897.
(40) Patil, V.; Singh, P.; Sonage, S.; Kumbhakarna, N.; Kumar, S. Experimental Investigation to Assess the Efficacy of Gasoline Surrogates with Engine Testing. Fuel **2022**, 324, 124493. https://doi.org/10.1016/j.fuel.2022.124493.
(41) Do, H.-Q.; Tran, L.-S.; Gasnot, L.; Mercier, X.; El Bakali, A. Experimental Study of the Influence of Hydrogen as a Fuel Additive on the Formation of Soot Precursors and Particles in Atmospheric Laminar Premixed Flames of Methane. Fuel **2021**, 287, 119517. https://doi.org/10.1016/j.fuel.2020.119517.
(42) NIST Standard Reference Database. NIST/EPA/NIH Mass Spectral Library. Available at <https://www.nist.gov/srd/nist-standard-reference-database-1a>.
(43) Van Geem, K. M.; Pyl, S. P.; Reyniers, M.-F.; Vercammen, J.; Beens, J.; Marin, G. B. On-Line Analysis of Complex Hydrocarbon Mixtures Using Comprehensive Two-Dimensional Gas Chromatography. J. Chromatogr. A **2010**, 1217 (43), 6623–6633. https://doi.org/10.1016/j.chroma.2010.04.006.
(44) Cieplik, M. K.; Epema, O. J.; Louw, R. Thermal Hydrogenolysis of Dibenzo-p-Dioxin and Dibenzofuran. Eur. J. Org. Chem. **2002**, 2002 (16), 2792–2799. https://doi.org/10.1002/1099-0690(200208)2002:16<2792::AID-EJOC2792>3.0.CO;2-H.
(45) Pecullan, M.; Brezinsky, K.; Glassman, I. Pyrolysis and Oxidation of Anisole near 1000 K. J. Phys. Chem. A **1997**, 101 (18), 3305–3316. https://doi.org/10.1021/jp963203b.
(46) Mackie, J. C.; Doolan, K. R.; Nelson, P. F. Kinetics of the Thermal Decomposition of Methoxybenzene (Anisole). J. Phys. Chem. **1989**, 93 (2), 664–670. https://doi.org/10.1021/j100339a033.
(47) Arends, I. W. C. E.; Louw, R.; Mulder, P. Kinetic Study of the Thermolysis of Anisole in a Hydrogen Atmosphere. J. Phys. Chem. **1993**, 97 (30), 7914–7925. https://doi.org/10.1021/j100132a020.
(48) Roy, S.; Askari, O. Detailed Kinetics for Anisole Oxidation under Various Range of Operating Conditions. Fuel **2022**, 325, 124907. https://doi.org/10.1016/j.fuel.2022.124907.
(49) CRECK modeling group: Anisole model. C1-C16 HT mechanism (Version 2003, March 2020). http://creckmodeling.chem.polimi.it/menu-kinetics/menu-kinetics-detailed-mechanisms/107-category-kinetic-mechanisms/402-mechanisms-1911-tot-ht (accessed 2023-04-11).
(50) Shi, X.; Wang, Q.; Violi, A. Chemical Pathways for the Formation of Benzofuran and Dibenzofuran in Combustion. Combust. Flame **2020**, 212, 216–233. https://doi.org/10.1016/j.combustflame.2019.10.008.
(51) Wiater, I.; Born, J. G. P.; Louw, R. Products, Rates, and Mechanism of the Gas-Phase Condensation of Phenoxy Radicals between 500-840 K. Eur. J. Org. Chem. **2000**, No. 6, 921–928. https://doi.org/10.1002/(SICI)1099-0690(200003)2000:6<921::AID-EJOC921>3.0.CO;2-P.
(52) Suzuki, S.; Kukkadapu, G.; Kiuchi, S.; Wagnon, S. W.; Kinoshita, K.; Takeda, Y.; Sakaida, S.; Konno, M.; Tanaka, K.; Oguma, M.; et al. Formation of PAHs, Phenol, Benzofuran, and Dibenzofuran in a Flow Reactor from the Oxidation of Ethylene, Toluene, and n-Decane. Combust. Flame **2022**, 241, 112136. https://doi.org/10.1016/j.combustflame.2022.112136.

(53) Bourgalais, J.; Carstensen, H.-H.; Herbinet, O.; Garcia, G. A.; Arnoux, P.; Tran, L.-S.; Vanhove, G.; Nahon, L.; Hochlaf, M.; Battin-Leclerc, F. Product Identification in the Low-Temperature Oxidation of Cyclohexane Using a Jet-Stirred Reactor in Combination with SVUV-PEPICO Analysis and Theoretical Quantum Calculations. J. Phys. Chem. A **2022**, 126 (34), 5784–5799. https://doi.org/10.1021/acs.jpca.2c04490.